The production and decay kinetics of ClOO in water and freon-11: A time-resolved resonance raman study
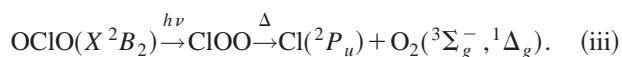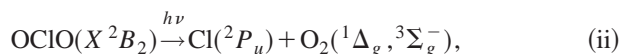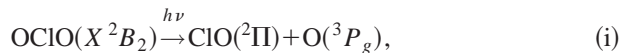
Sophia C. Hayes, Carsten L. Thomsen,[a] and Philip J. Reid[b]
Box 351700, Department of Chemistry, University of Washington, Seattle, Washington 98195

The production of ClOO following OClO photolysis in water and fluorotrichloromethane (freon-11) is investigated using time-resolved resonance Raman (TRRR) spectroscopy. Stokes spectra are obtained as a function of time following OClO photoexcitation using pump and probe wavelengths of 390 and 260 nm, respectively. Scattering assignable to ClOO is observed, and appears with a time constant of 27.9 ± 4.5 ps in water and 172 ± 30 ps in freon-11. The ClOO intensity decays with a time constant of $\sim398\pm50$ ps in water and 864 ± 200 ps in freon-11. Although the production and decay kinetics are solvent dependent, the quantum yield for ClOO production is similar between water and freon-11. Femtosecond pump–probe studies designed to monitor the evolution in optical density at 390 and 260 nm following OClO photoexcitation are also presented. These studies demonstrate that geminate recombination of the primary photoproducts is less efficient in freon-11 relative to water. This result taken in combination with the solvent invariance of the ClOO-production quantum yield indicates that ClOO is not formed via geminate recombination. Instead, the results presented here suggest that OClO photoisomerization results in the production of ClOO. Finally, the vibrational energy content of ClOO upon internal conversion to the ground state is studied through comparison of the ClOO Raman and absorption cross sections to those predicted using computational methods. These studies suggest that ground-state ClOO is produced with minimal excess vibrational energy. The results presented here provide new insight into the mechanism of ClOO formation following OClO photoexcitation. © *2001 American Institute of Physics.* [DOI: 10.1063/1.1418733]

I. INTRODUCTION

The photochemistry of chlorine dioxide (OClO) has been of recent interest due to its participation in stratospheric photochemistry, and its role as an indicator of stratospheric chlorine activation.[1–3] The following reaction channels are available to OClO following photoexcitation:

$$OClO(X\,^2B_2)\xrightarrow{h\nu}ClO(^2\Pi)+O(^3P_g),\qquad\text{(i)}$$

$$OClO(X\,^2B_2)\xrightarrow{h\nu}Cl(^2P_u)+O_2(^1\Delta_g,^3\Sigma_g^-),\qquad\text{(ii)}$$

$$OClO(X\,^2B_2)\xrightarrow{h\nu}ClOO\xrightarrow{\Delta}Cl(^2P_u)+O_2(^3\Sigma_g^-,^1\Delta_g).\qquad\text{(iii)}$$

The quantum yield for chlorine production (Φ_{Cl}) is dependent on phase $\Phi_{Cl}=0.04$ in the gas phase and increases to unity in low-temperature matrixes.[1,4–7] Aqueous solutions demonstrate intermediate behavior with $\Phi_{Cl}=0.1$.[8–10] In addition, recent pump–probe studies of aqueous OClO have shown that $\sim20\%$ of Cl is produced via ClOO decomposition.[11]

ClOO has proven to be an elusive target for study. Porter and Wright first proposed that ClOO was produced as an intermediate in flash-photolysis studies of chlorine–oxygen mixtures.[12] Later photochemical studies of OClO isolated in low-temperature matrixes provided the first spectroscopic information on ClOO.[6,13] In particular, Arkell and Schwager performed a definitive spectroscopic analysis of matrix-isolated ClOO generated from isotopically labeled OClO.[6] In this study, infrared absorptions at 1441, 407, and 373 cm^{-1} were observed and assigned to O–O stretching, Cl–O stretching, and the valence bend transitions of ClOO, respectively. Subsequent matrix-isolation studies provided a refinement of these assignments, largely motivated by the observation of a transition at 200 cm^{-1}.[7] In this later work, transitions at 200 and 373 cm^{-1} were assigned to the fundamental and overtone of the Cl–O stretch, and the 407 cm^{-1} transition was assigned to the bend fundamental.[7,14] Production of ClOO has also been observed in ice.[15] Finally, recent time-resolved resonance Raman studies[16] and femtosecond absorption studies[11] have provided the first definitive evidence for ClOO formation in aqueous solution.

Although it has been shown that ClOO is produced following OClO photolysis, the mechanism by which this isomer is formed remains unclear. There are two proposed mechanisms for ClOO formation: OClO photoisomerization and geminate recombination of the primary photofragments. In photochemical studies of gaseous OClO by Vaida and co-workers, photoisomerization was invoked to explain resonances observed in the REMPI spectra of Cl produced following OClO photoexcitation.[17,18] Solution-phase studies have also been largely interpreted in terms of the photoisomerization model.[8,11,16,19] In contrast, studies in low-

J. Chem. Phys., Vol. 115, No. 24, 22 December 2001

Decay kinetics of ClOO in water   11229

temperature matrixes and on ice surfaces have used both the photoisomerization and geminate recombination models to explain ClOO production in these environments.[6,7,15,20,21] Finally, theoretical studies of OClO and ClOO by Gole provided a plausible mechanism for OClO photoisomerization;[22] however, later computational studies by Peterson and Werner were not supportive of this model.[14,23,24] To date, the mechanism of ClOO production remains unclear.

To study the mechanism of ClOO formation, we have performed two-color, time-resolved resonance Raman (TRRR) studies of OClO dissolved in water and trichlorofluoromethane (freon-11). The production of ClOO following OClO photoexcitation at 390 nm is followed using resonance Raman spectra obtained with a 260-nm probe beam. Freon-11 was chosen for study since it is an aprotic solvent in which the absence of self-association via hydrogen bonding is anticipated to provide for a weaker solvent cage and a corresponding reduction in geminate recombination efficiency relative to water.[25,26] Previous TRRR studies of similar motivation were performed in acetonitrile;[26] however, this solvent could not be employed here due to spectral overlap with ClOO. We find that ClOO is produced in both solvents, and that the appearance and decay kinetics of this species are solvent dependent. Specifically, aqueous ClOO appears and decays with time constants of 27.9 ± 4.5 ps and 398 ± 50 ps, respectively, where the kinetics in freon-11 is much slower with corresponding time constants of 172 ± 30 ps and 864 ± 200 ps. Although the appearance and decay kinetics are solvent dependent, the quantum yield for ClOO production is solvent independent. Femtosecond pump probe studies at 390 and 260 nm are presented which demonstrate that geminate recombination of the primary photoproducts is threefold less efficient in freon-11 relative to water. The solvent independence of the ClOO production quantum yield combined with the substantial reduction in geminate-recombination efficiency in freon-11 suggests that ClOO is not produced by primary-photoproduct recombination. Instead, the results presented here are interpreted in terms of OClO photoisomerization, and a detailed description of this process is outlined. Finally, computational studies are outlined that investigate the vibrational energy content of ground-state ClOO. Comparison of the computational and experimental Raman and absorption cross sections suggests that ground-state ClOO is produced with limited excess vibrational energy. In total, the results presented here provide new information regarding the mechanism of ClOO formation following OClO photoexcitation.

II. EXPERIMENTAL METHODS

The laser system employed in these studies has been described elsewhere.[10,26–28] An argon–ion laser (Spectra Physics 2065-07) operating all-lines was used to pump a homebuilt Ti:Sapphire oscillator that produced 30-fs pulses (full width at half maximum) centered at 780 nm at a repetition rate of 91 MHz. The oscillator output was temporally elongated using an optical stretcher and delivered to a Ti: Sapphire regenerative amplifier (Clark-MXR CPA-1000-PS) equipped with independently tunable single- and double-plate birefringent filters to constrain the amplifier bandwidth.

The amplifier output following compression consisted of 600-fs, 700-μJ pulses centered at 780 nm at a repetition rate of 1 kHz. Frequency doubling of the amplifier output using a 200-μm thick β-BBO crystal (type I) produced the 390-nm pump beam. The 260-nm probe beam was generated by sum-frequency mixing a portion of the 390-nm beam with residual fundamental in a 200-μm thick β-BBO crystal (type II). The probe beam waist at the sample was reduced to half that of the pump to ensure spatial overlap. The contribution of rotational dynamics to the data was minimized by rotating the polarization of the pump to 54.7° relative to the probe using a zero-order half-wave plate.

Time-resolved resonance Raman (TRRR) spectra were obtained as follows. The pump and probe beams were focused onto a fused-silica flow cell containing 20-mM solutions of OClO in distilled water or fluorotrichloromethane (freon-11, Aldrich). A 135° backscattering geometry was employed, with the scattered light collected and delivered to a 0.5-m focal-length spectrograph (Acton 505F) using standard, UV-quality refractive optics. The spectrograph was equipped with a 3600-grooves/mm holographic grating, and spectrometer slit widths were adjusted to provide 15 cm^{-1} resolution. The scattered light was detected by a LN$_2$-cooled, 1340×100 pixel, back-thinned CCD detector (Princeton Instruments). Overlap between the pump and probe was optimized by monitoring the transient absorption of the probe using an ultraviolet-enhanced photodiode (Advanced Photonix, Inc. SD 200-13-23-242) located behind the sample. Raman spectra with the ''probe-only,'' the ''pump-and-probe,'' and the ''pump-only'' incident on the sample were obtained at each time delay. The pump-only spectrum was directly subtracted from the pump-and-probe spectrum to produce the ''probe-with-photolysis'' spectrum. Since the experiment is performed with different pump and probe wavelengths, background scattering due to the pump is extremely modest and makes only a minor contribution to the pump-and-probe spectrum. The probe-only spectrum was directly subtracted from the probe-with-photolysis spectrum to produce the difference spectra reported here. Three sets of 30 min integrations were performed for each configuration of the pump and probe at a given delay, and three difference spectra were summed together at each time point to construct the spectra presented here. When measuring kinetics, 12 min (water) or 18 min (freon-11) integrations were performed for each pump-probe configuration. Pulse energies were 12 and 2 μJ for the pump and probe, respectively. The scattered intensity was found to be linearly dependent on both pump and probe power. The instrument response as measured by the optical Kerr effect in water was 1.2 ± 0.1 ps. The sample absorption spectrum before and after an experiment was identical within experimental error, demonstrating that sample degradation had not occurred during the experiment. The preparation of OClO has been reported elsewhere.[29,30]

To determine the ClO and O primary photoproducts recombination quantum yield in freon-11, subpicosecond pump–probe studies were performed where the evolution in optical density at 390 and 260 nm was monitored as a function of time following OClO photoexcitation. The methodology employed in these studies has been described in detail

elsewhere.[27] Optical-density evolution was monitored for time delays up to 800 ps. To maintain beam overlap over such large displacements of the optical delay line, the pump beam waist was enlarged to ~5 times that of the probe. The goodness of spatial overlap was evaluated by monitoring the pump beam as it passed through a pinhole while the delay was altered. This measurement established that the error in absolute optical-density change due to spatial drift was <10% of the overall change in optical density measured at a given probe wavelength.

The absolute resonance Raman scattering cross sections for the 1650 cm^{-1} transition of water at 252 and 266 nm were obtained using a Nd:YAG-laser (Spectra-Physics GCR-170)-based spectrometer described in detail elsewhere.[30] In addition to intensities, the depolarization ratio of this transition, defined as the intensity of scattered light with polarization perpendicular to that of the incident radiation divided by the intensity of scattered light with parallel polarization, was also determined using previously reported methods.[29]

III. COMPUTATIONAL METHODS

In recent pump–probe studies of aqueous OClO, transient absorption spectra between 200 and 400 nm were acquired at various times following photoexcitation, and it was proposed that the spectral evolution observed between time delays of 20 and 50 ps from 220 to 240 nm was due to ClOO vibrational relaxation.[11] This assignment was consistent with our earlier TRRR studies where an increase in ClOO intensity at early times was assigned to cross-section enhancement accompanying ground-state vibrational relaxation.[16] In order to further characterize the temperature-dependent absorption and resonance Raman cross section of ClOO, and to ascertain the vibrational energy content of the molecule following its production, we have modeled the absorption and Raman cross sections of ClOO using the time-dependent formalism.[31] In this formalism, the absorption (σ_A) and Raman (σ_R) cross sections are given by

$$\sigma_A(E_l,T) = \frac{4\pi e^2 E_l M_{eg}^2}{6\hbar^2 cn} \sum_i P_i \int_{-\infty}^{\infty} \langle i|i(t)\rangle$$
$$\times \exp\left[\frac{i(E_l+E_i)t}{\hbar}\right] D(t)dt, \qquad (1)$$

$$\sigma_R(E_l,T) = \frac{8\pi e^4 E_l E_s^3 M_{eg}^4}{9\hbar^6 c^4} \sum_i P_i$$
$$\times \left| \int_0^{\infty} \langle f|i(t)\rangle \exp\left[\frac{i(E_l+E_i)t}{\hbar}\right] D(t)dt \right|^2. \qquad (2)$$

In the above equations, M_{eg} is the transition moment, n is the index of refraction, E_l is the energy of the incident radiation, and E_s is the energy of the scattered radiation. $D(t)$ is the homogeneous linewidth composed of both pure dephasing and population decay. A Gaussian exponential form for $D(t)$ was found to best reproduce the red edge of the absorption spectrum. It should be noted that the homogeneous linewidth was taken to be independent of excess vibrational energy.

The $\langle i|i(t)\rangle$ term in Eq. (1) represents the time-dependent overlap of the initial state with the same state propagating under the influence of the excited-state Hamiltonian. Similarly, the $\langle f|i(t)\rangle$ term in Eq. (2) represents the time-dependent overlap of the final state in the Raman-scattering process with the initial state propagating under the influence of the excited-state Hamiltonian. Finally, summation over the occupation probabilities P_i of vibrational states (denoted by i) is performed. This summation is required due to the population of levels up to $i=5$ along low-frequency coordinates (200 and 428 cm^{-1}) at 298 K, and is also necessary to perform cross-section calculations at higher molecular temperatures.

The absorption and Raman time correlators (e.g., $\langle i|i(t)\rangle$ and $\langle f|i(t)\rangle$) are multidimensional functions representing the product of overlaps along each vibrational normal coordinate. Assuming coordinate separability, the absorption and Raman time correlators become the product of single-mode overlaps.[32] In these calculations, the simple-harmonic approximation was used for the O–O stretch and bend in which ground-and excited states are modeled as harmonic surfaces of equal frequency. Overlaps along these coordinates were determined using the analytic expressions reported by Mukamel and co-workers.[33] *Ab initio* studies of ClOO suggest that the optically accessed excited states are dissociative along the Cl–O coordinate.[34] Therefore, the overlap along this coordinate was determined using a linear dissociative potential, and propagation on this surface was performed using the approximate method of Feit and Fleck.[35,36] In this approach, $|i(t)\rangle$ is given by

$$|i(t)\rangle = e^{[i(\Delta t)\nabla^2]/4M} e^{-i(\Delta t)V} e^{[i(\Delta t)\nabla^2]/4M}|i(0)\rangle + \vartheta(\Delta t^3), \qquad (3)$$

where ∇^2 is the Laplacian in position space, V is the excited-state linear dissociative potential, $V=\beta q$ [with $\beta=\delta V/\delta q$ (in cm^{-1})], Δt is the size of the propagation time step, and q represents displacement along the dimensionless normal coordinate. A 0.1-fs time step was employed, and overlaps were calculated up to 100 fs. The dissociative overlaps calculated by the approximate-time propagator method were compared to corresponding analytic expressions for $i=0$, 1, and 2,[32,37] and identical results were obtained. Overlaps in which $i>2$ were studied, and such overlaps are more easily determined using the approximate time-propagator method. For studies in which the evolution of the Raman and absorption cross sections with excess temperature were investigated, vibrational energy was assumed to be distributed in accord with Boltzmann statistics. The time-dependent overlaps and corresponding absorption and Raman cross sections were calculated for every ground-state configuration for which the occupation probability was ≥1×10^{-5}. At the highest temperatures investigated (2000 K), this probability cutoff allowed for inclusion of >99% of the ground-state population.

IV. EXPERIMENTAL RESULTS

Figure 1 presents the time-resolved resonance Raman (TRRR) Stokes difference spectra of aqueous OClO obtained using pump and probe wavelengths of 390 and 260 nm, re-
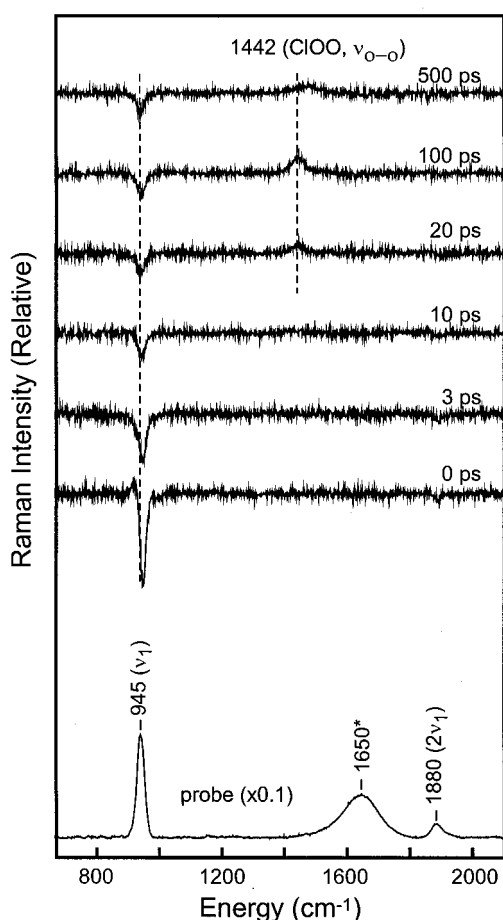
FIG. 1. Time-resolved resonance Raman Stokes difference spectra of aqueous OClO. Data were obtained using 390 and 260-nm pump and probe fields, respectively. The temporal delay between the pump and the probe at which a given spectrum was obtained is indicated. The probe-only spectrum is presented at the bottom of the figure. The transition marked with an asterisk in the probe-only spectrum is the fundamental of the water bend.

FIG. 2. (A) Intensity of the aqueous OClO symmetric stretch transition (945 cm^{-1}) as a function of pump–probe delay. Data were best fit by a sum of three exponentials convolved with the instrument response resulting in recovery times of 0.15 ± 0.1 ps (instrument-response limited), 5.7 ± 1.5 ps, and a long-time offset (time constant fixed to 10 000 ps) representing residual depletion. The short dashed line is the instrument response (1.2 ± 0.1 ps). (B) Intensity of the ClOO O–O stretching transition at 1442 ± 2 cm^{-1} in water as a function of time delay. The data were fit by a sum of two exponentials convolved with the instrument response resulting in appearance and decay time constants of 27.9 ± 4.5 ps and 398 ± 50 ps, respectively. In addition, inclusion of a 12.7 ± 1.5 ps dwell relative to zero time was necessary to reproduce the data. (C) Intensity of the ClOO O–O stretching transition at 1436 cm^{-1} (ν_{OO}) in freon-11 as a function of time delay. The data were fit by a sum of two exponentials convolved with the instrument response resulting in appearance and decay time constants of 172 ± 30 ps and 864 ± 200 ps, respectively. In addition, inclusion of a 13 ± 0.4 ps dwell relative to zero time was necessary to reproduce the data.

spectively. At 0 ps, when the pump and the probe are overlapped in time, negative intensity is observed for transitions corresponding to OClO consistent with photoinitiated depletion of the ground state. Comparison of the negative 945-cm^{-1} intensity in the 0-ps spectrum to that in the probe-only spectrum establishes that ~6% depletion of ground-state OClO occurs under the conditions employed. As the delay between the pump and probe is increased, the OClO depletion decreases, consistent with reformation of ground-state OClO via geminate recombination of the primary photofragments. After 20 ps, the scattering depletion remains constant at a value of $20\pm10\%$, relative to that at 0 ps. Identical behavior was observed in our previous TRRR studies performed at 390 nm.[26] The temporal evolution of the OClO symmetric-stretch fundamental transition intensity (945 cm^{-1}) is presented in Fig. 2(A). These data were best fit by a sum of three exponentials convolved with the instrument response resulting in recovery times of 0.15 ± 0.1 ps (i.e., instrument-response limited), 5.7 ± 1.5 ps, and a long-time offset (time constant fixed to 10 000 ps) representing persistent depletion.

The spectra presented in Fig. 1 demonstrate that ClOO is produced following the photolysis of aqueous OClO. Spe-
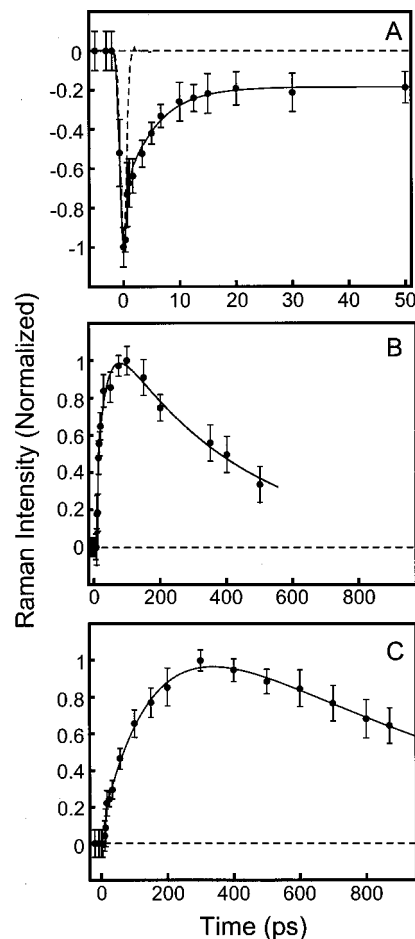
cifically, the positive intensity observed at 1442 cm^{-1} corresponds to the O–O stretch of ClOO.[6,7,20,38] To solidify this assignment, TRRR spectra at lower frequency were obtained, and intensity corresponding to the ClOO bend was observed. Figure 3 presents Stokes difference spectra obtained 3 and 100 ps after photolysis of OClO. At 100 ps, intensity at 428 and 1442 cm^{-1} is evident corresponding to the bend and O–O stretch, respectively. We have not been able to observe the Cl–O stretch fundamental at 200 cm^{-1} due to Rayleigh scatter. To determine the kinetics of ClOO production and decay, the temporal evolution of the 1442 cm^{-1} transition was plotted as a function of time [Fig. 2(B)]. The data presented in Fig. 1 indicate that ClOO production is signifi-
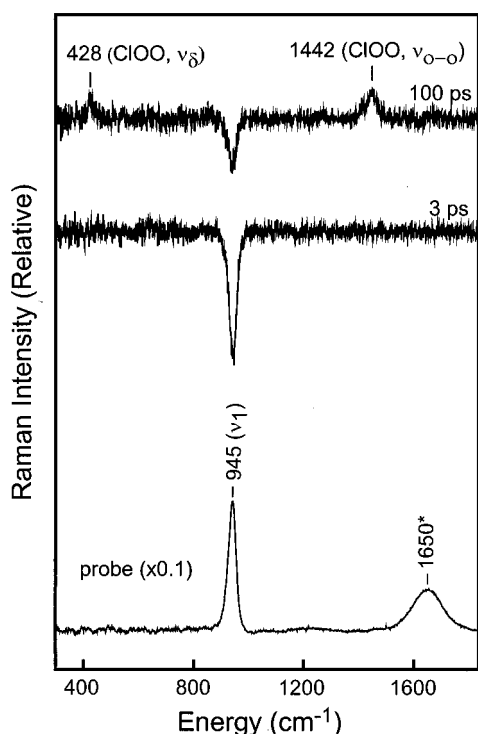
FIG. 3. Time-resolved resonance Raman Stokes difference spectra of aqueous OClO at lower frequency. The time delay between the pump and the probe is indicated for each spectrum. The probe-only spectrum is also presented with solvent transitions marked with an asterisk. Two modes of ClOO are apparent, the O–O stretch at 1442 cm^{-1} and the bend at 428 cm^{-1} as discussed in the text.

FIG. 4. Time-resolved pump–probe dynamics of OClO in (A) water and (B) freon-11 with pump and probe wavelengths of 390 nm. The instrument response was 1.2 ± 0.1 ps. (A) The solid line represents the best fit to a sum of three exponentials convolved with the instrument response resulting in time constants (with normalized amplitudes in parentheses) of 6.5 ± 0.9 ps (-0.93), 251 ± 151 ps (-0.06), and a long-time offset (time constant fixed to 10 000 ps) representing residual depletion (-0.01). (B) The solid line represents the best fit to a sum of three exponentials convolved with the instrument response resulting in time constants (with normalized amplitudes in parentheses) of 96.6 ± 15.6 ps (-0.09), 5167 ± 1602 ps (0.38), and a long-time offset (time constant fixed to 10 000 ps) representing residual depletion (-0.53).

cantly delayed relative to OClO reformation with the intensity of the O–O stretch reaching a maximum at ∼100 ps. Consistent with this observation, best fit to these data by a sum of two exponentials convolved with the instrument response corresponds to appearance and decay time constants of 27.9 ± 4.5 and 398 ± 50 ps, respectively. In addition, best fit to the data necessitated an additional delay of 12.5 ps relative to zero time.

As mentioned in the Introduction, the absence of intermolecular hydrogen bonding in freon-11 is expected to produce a solvent cage that is more labile to escape of the primary photoproducts. To determine if cage escape in this solvent is less efficient relative to water, the geminate-recombination quantum yield in freon-11 was determined. Specifically, the evolution in optical density following OClO photoexcitation at 390 nm was monitored at this same wavelength and compared to the corresponding evolution observed in water (Fig. 4). OClO dominates the optical-density evolution at this probe wavelength; therefore, these data provide a measure of photoinitiated ground-state OClO depletion and subsequent recovery via geminate recombination. Following photoexcitation, an initial reduction in optical density is observed in both solvents consistent with ground-state depletion via photolysis. The initial depletion is followed by a recovery in optical density corresponding to the reappearance of ground-state OClO. In water [Fig. 4(A)], 90% of the optical density recovers within 30 ps, with a small, later time (>100 ps) increase in optical density also occurring due to the formation of the Cl–water charge–
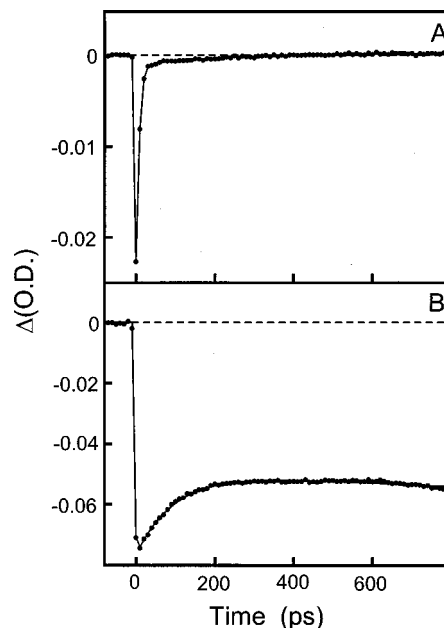
transfer complex through ClOO decomposition.[11] The evolution in optical density for water was fit to a sum of three exponentials convolved with the instrument response, resulting in time constants (with normalized amplitudes in parentheses) of 6.5 ± 0.9 ps (-0.93), 251 ± 151 ps (-0.06), and a long-time offset (time constant fixed to 10 000 ps) representing residual depletion (-0.01). In freon-11, a large persistent depletion in optical density is observed at 390 nm [Fig. 4(B)] in contrast to the extensive recovery observed in water. Direct comparison of the optical-density evolution in water and freon-11 is complicated by the fact that the absorption spectrum of the Cl–freon charge–transfer complex is ∼10-nm blueshifted relative to the Cl–water complex.[39] However, the absorption cross section of the Cl–freon charge–transfer complex is negligible at wavelengths greater than ∼360 nm such that the recovery in optical density at 390 nm provides a direct measure of ground-state OClO production. Therefore, the results presented in Fig. 4(B) establish that the geminate recombination quantum yield is 0.3 ± 0.1 in freon-11, substantially reduced relative to water. The optical-density evolution was fit to a sum of three exponentials convolved with the instrument response resulting in time constants (with normalized amplitudes in parentheses) of 96.6 ± 15.6 ps (-0.09), 5167 ± 1600 ps (0.38), and a long-time offset (time constant fixed to 10 000 ps) representing residual depletion (-0.53). The ∼5-ns time constant must be
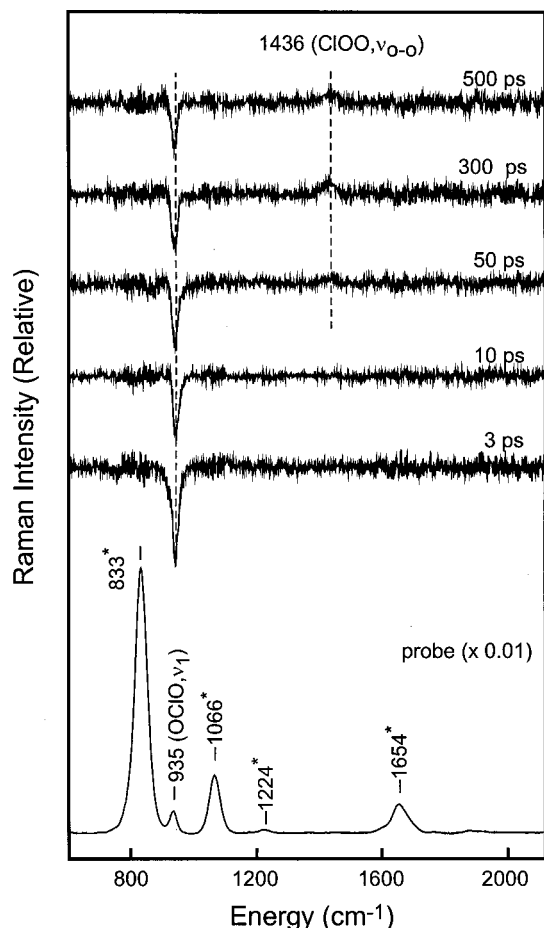
FIG. 5. Time-resolved resonance Raman Stokes difference spectra of OClO dissolved in freon-11. The temporal delay between the pump and the probe for a given spectrum is indicated. The probe-only spectrum is presented at the bottom of the figure. The transitions marked with an asterisk in the probe-only spectrum are due to the solvent.
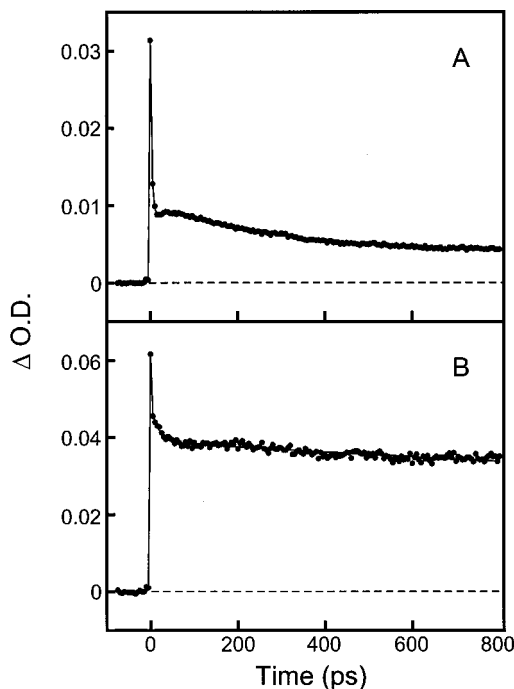

FIG. 6. (A) Time-resolved pump–probe dynamics of OClO in water with pump and probe wavelengths of 390 and 260 nm, respectively. The data were fit by a sum of four exponentials convolved with the instrument response resulting in time constants (with normalized amplitudes in parentheses) of 3.3 ± 0.4 ps (0.6), 21.5 ± 11.2 ps (-0.1), 284 ± 70 ps (0.17), and a long-time offset (time constant fixed to 10 000 ps) representing residual offset in optical density. (B) Time-resolved pump–probe dynamics of OClO in freon-11. The data were fit by a sum of four exponentials convolved with the instrument response resulting in time constants (with normalized amplitudes in parentheses) of 0.7 ps (0.25), 17.95 ± 2.87 ps (0.10), 323 ± 166 (0.05) and a long-time offset (time constant fixed to 10 000 ps) representing residual offset in optical density.

viewed as a very rough estimate, given the limited delay times investigated here.

To investigate the role of geminate recombination in ClOO production, we performed TRRR studies in freon-11. TRRR Stokes difference spectra of OClO in freon-11 are presented in Fig. 5. Similar to the behavior observed in water, negative intensity for OClO transitions is observed corresponding to ground-state depletion by photolysis. The depletion in OClO intensity evident at later delays is significantly greater than in water, demonstrating that geminate recombination is much less efficient in this solvent consistent with the pump–probe results presented above. ClOO production in freon-11 is also observed; however, the appearance of this species occurs on a significantly slower time scale relative to water. Figure 2(C) presents the temporal evolution in the scattering intensity for the 1436 cm^{-1} transition of ClOO in freon-11. The data were best fit by a sum of two exponentials convolved with the instrument response resulting in appearance and decay time constants of 172 ± 30 and 864 ± 200 ps, respectively. In addition, best fit necessitated the introduction of a 13 ± 0.4 ps delay relative to zero time, similar to the behavior observed in water.

Figure 6 presents the pump–probe dynamics of OClO in

water and freon-11 observed at 260 nm following photoexcitation at 390 nm. The aqueous OClO results [Fig. 6(A)] are essentially identical to those reported by Thomsen et al.[11] These authors convincingly demonstrated that the evolution in optical density at this wavelength is dominated by the formation and decay of ClOO and ClO. Given that cage escape of the primary photofragments is more efficient in freon-11, we would expect to observe an increase in ClO production in this solvent. Therefore, these pump–probe measurements provide a critical check of geminate-recombination quantum yields defined above. The substantial increase in long-time optical density observed in freon-11 as compared to water is consistent with increased ClO concentration, and demonstrates that the geminate-recombination quantum yield is substantially reduced in freon-11. The evolution in optical density observed in water [Fig. 6(A)] was fit by a sum of four exponentials convolved with the instrument response resulting in time constants (with normalized amplitudes in parenthesis) of 3.3 ± 0.4 ps (0.62), 21.5 ± 11.2 ps (-0.11), 284 ± 70 ps (0.17), and a long-time offset (time constant fixed to 10 000 ps) representing residual absorption (0.10). The optical density evolution in freon-11 [Fig. 6(B)] was also fit by a sum of four exponentials convolved with the instrument response resulting in decay time constants of 0.7 ± 0.4 ps (0.25), 18.0 ± 2.9 ps (0.10), 323 ± 166 ps (0.05), and

a long-time offset (time constant fixed to 10 000 ps) representing residual absorption (0.59).

A. Relative ClOO quantum yield

To determine if the quantum yield for ClOO formation is solvent dependent, experiments were performed in which the relative ClOO production quantum yields in water and freon-11 were determined. Since the appearance and decay kinetics of ClOO are solvent dependent, any determination of the ClOO formation quantum yield must compare delay times where the ClOO concentration is at a maximum. The intensity of the O–O stretch of ClOO reaches a maximum at ~100 ps in water and at ~300 ps in freon-11. Assuming that the intensity of this transition at these two time delays represents the maximum ClOO concentration in each solvent, a comparison of intensities at these delays provides a relative measure of the ClOO quantum yields. To accurately perform this comparison, we obtained TRRR difference spectra of OClO in water and freon-11 at these two time delays on the same day, and by interchanging samples between experiments to minimize variations in intensity due to differences in alignment. The ClOO scattered intensity was found to be equivalent in freon-11 and water within experimental error ($\pm 20\%$). Given the differences in production and decay time constants, equivalent intensity does not necessarily mean that the ClOO production quantum yield is solvent independent. However, a check of the expected ClOO concentration profiles employing the time constants determined above in conjunction with a sequential reaction mechanism demonstrates that similar ClOO intensities are indeed expected at 100- and 300-ps delay in water and freon-11, respectively, if the ClOO quantum yield is independent of solvent. Therefore, the similarity in maximum ClOO scattering intensity demonstrates that the quantum yield of ClOO production is similar between these two solvents.

V. COMPUTATIONAL RESULTS

To assist in interpreting the evolution in intensity observed in the femtosecond pump–probe and TRRR studies, a computational study was undertaken to characterize the temperature dependence of the ClOO absorption and resonance Raman cross sections. The ClOO absorption spectrum presented in Fig. 7(A) corresponds to the gas-phase spectrum observed at 191 K,[40] but shifted 10 nm to longer wavelengths to coincide with the absorption spectrum of ClOO on ice.[15] The absolute Raman cross sections for the O–O stretch and bend transitions of aqueous ClOO were determined as follows. First, the ClOO concentration was obtained by comparing the ClOO scattering intensity at 100 ps to the negative OClO intensity at 945 cm^{-1} in the 0-ps spectrum, which represents 6% depletion of the ground state (see above). In addition, pump–probe studies have established that the quantum yield for ClOO production is 0.02 ± 0.01.[11] Using the quantum yield for ClOO production and the extent of OClO ground-state depletion, a ClOO concentration of $2.4\pm1.2 \times 10^{-5}$ M is determined.

Measurement of the ClOO absolute scattering cross sections can be performed through comparison to the intensity of OClO symmetric-stretch fundamental transition (945
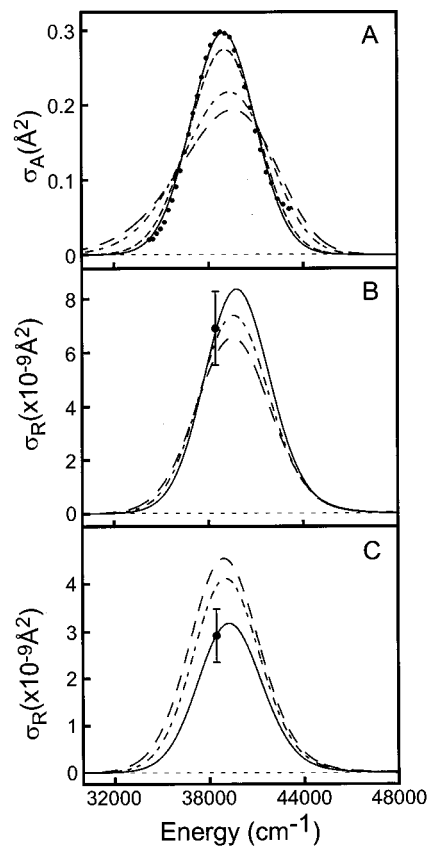

FIG. 7. (A) The absorption spectrum of ClOO (points) (Ref. 40). Spectrum is shifted to longer wavelengths by 10 nm relative to the literature spectrum to agree with the absorption spectrum of ClOO on ice as reported by Pursell and co-workers (Ref. 15). The solid line is the fit to the absorption as described in the text. Also included are the calculated absorption spectra for molecular temperatures of 298 K (small dash), 700 K (dot dash), and 1000 K (long dash). (B) Calculated Raman excitation profiles for the ClOO O–O stretch fundamental and (C) bend fundamental transitions as a function of temperature. The points represent the experimentally determined Raman cross sections measured using 260-nm excitation. The curves correspond to molecular temperatures of 298 K (solid), 700 K (dot-dash), and 1000 K (long dash).

cm^{-1}) in the probe-only spectrum. However, the absolute Raman cross section for this transition at 260 nm has not been reported; therefore, this cross section was determined by comparison to the water bend fundamental at 1650 cm^{-1} using the following:

$$\frac{\sigma_{OClO}}{\sigma_{water}} = \frac{I_{OClO} C_{water}[(1+2\rho)/(1+\rho)]_{water}}{I_{water} C_{OClO}[(1+2\rho)/(1+\rho)]_{OClO}}. \tag{4}$$

In the above expression, c_i is the concentration of the molecule of interest and ρ is the depolarization ratio. Depolarization ratios for both the water OH–stretch and bend fundamental transitions have been reported,[41,42] as have the OH–stretch fundamental transition cross sections from 200 to 266 nm.[41] However, the absolute Raman cross section of the bend at 260 nm has not been reported. Therefore, this cross section was determined at 252 and 266 nm by comparison to the OH–stretch fundamental transition. The depolarization ratio for the bend transition was measured at 266 nm and

J. Chem. Phys., Vol. 115, No. 24, 22 December 2001

Decay kinetics of ClOO in water   11235

TABLE I. $^2A'$ excited-state potential energy surface parameters for ClOO. Non-mode-specific parameters used to calculate the absorption and Raman cross sections: $\Gamma = 1000 \pm 10$ cm^{-1}, $M_{eg} = 0.74$ Å, $E_{00} = 38\,500$ cm^{-1}, and $n = 1.35$.

Transition[a]	ω_g (cm^{-1})[b]	ω_e (cm^{-1})	Δ[c]	σ_R calc($\times 10^{-9}$ Å^2)	σ_R exp($\times 10^{-9}$ Å^2)
ν_{OO}	1442	1442	0.53	6.75	6.90 ± 1.38
ν_δ	428	428	0.97	2.92	2.91 ± 0.58
ν_{ClO}	200	d	⋯	34.7	⋯
$2\nu_{ClO}$	⋯	⋯	⋯	8.86	⋯

[a]Raman transition for which cross-section calculations were performed. The symbols ν_{OO}, ν_δ, and ν_{ClO} refer to the O–O stretch, bend, and ClO stretch, respectively.

[b]ω_g refers to the ground-state harmonic frequency, and ω_e is the excited-state harmonic frequency. Vibrational frequencies are those observed in the matrix isolation study of Müller and co-workers (Ref. 7).

[c]Dimensionless displacement of the excited-state potential energy surface minimum relative to the ground state.

[d]The slope of the linear dissociative excited-state potential energy surface along the Cl–O stretch used in the calculation was 1500 cm^{-1}.

found to be 0.54 ± 0.04, similar to the 0.57 value determined by Moskovits *et al.* at 514 nm, suggesting that the depolarization ratio of the bend is relatively independent of wavelength over this spectral region. Similar behavior has been observed for the OH stretch ($\rho_{OH} = 0.19$).[41] The reported cross section for the OH stretch at 266 nm (3.09×10^{-11} Å^2) was used, while the cross section for this transition at 252 nm (3.99×10^{-11} Å^2) was determined using the reported A-term fit parameters.[41] With these cross sections, the absolute Raman cross sections for the bend fundamental transition at 252 and 266 nm were determined to be $2.14 \pm 0.15 \times 10^{-13}$ Å^2 and $1.49 \pm 0.32 \times 10^{-13}$ Å^2, respectively. The A-term fit for the OH stretch between 252 and 266 nm is essentially linear, and if we assume that similar behavior characterizes the bend, linear extrapolation results in a bend scattering cross section of $1.76 \pm 0.32 \times 10^{-13}$ Å^2 at 260 nm. With this cross section, the absolute Raman cross section for the OClO symmetric-stretch fundamental transition was determined to be $2.90 \pm 0.53 \times 10^{-10}$ Å^2.[43] Finally, the absolute Raman cross sections for the O–O stretch and bend modes of ClOO were determined to be $6.90 \pm 1.38 \times 10^{-9}$ Å^2 and $2.91 \pm 0.58 \times 10^{-9}$ Å^2, respectively. These values are assumed to correspond to a molecular temperature of 298 K since they were obtained from the 100-ps TRRR difference spectrum at which time vibrational relaxation of ClOO is considered complete (see below).

The absorption and the absolute Raman cross sections of ClOO were simultaneously reproduced using Eqs. (1) and (2). Best reproduction of the absorption spectrum is shown as the solid line in Fig. 7(A), and corresponding fits to the O–O stretch and bend cross sections are presented as the solid lines in Figs. 7(B) and 7(C), respectively. The parameters used in these calculations are provided in Table I. The slope of the linear dissociative excited-state potential along the Cl–O coordinate was 1500 cm^{-1}, remarkably consistent with the computational results of Jafri *et al.*[34] In addition, a large homogeneous linewidth was necessary to restrict the amplitude of the Raman cross section for the Cl–O stretch overtone transition, consistent with the lack of observation of either this or the fundamental transition in the difference spectra. Finally, the absorption spectrum and the Raman excitation profiles (REPs) for the O–O stretch and bend fundamental transitions of ClOO were determined as a function of

temperature up to 2000 K. However, temperatures over 1000 K would lead to decomposition of the molecule given the dissociation barrier along the Cl–O stretch of only 20.2 kJ.[44] The absorption spectrum [Fig. 7(A)] demonstrates "typical" behavior, with the breadth of the absorption band increasing with an increase in temperature. Interestingly, the REPs for the O–O stretch [Fig. 7(B)] and bend [Fig. 7(C)] demonstrate very different temperature dependence. The REP for the bend increases in intensity and broadens to both the low and high frequency accompanied by a slight shift to low frequencies [Fig. 7(C)]. In contrast, the REP for the O–O stretch shows a small reduction in intensity with an increase in temperature. Most important is the predicted slight evolution of the scattering cross section for this transition at 260 nm ($\sim$13% decrease from 298 to 1000 K). This result suggests that the increase in O–O scattering evident in the TRRR data reflects predominantly a change in ground-state population rather than an evolution in vibrational temperature.

Figure 7(A) demonstrates that the absorption spectrum of ClOO is very sensitive to temperature, and suggests that transient absorption spectra can be used to ascertain vibrational energy content of this species. In the recent pump–probe studies of Thomsen *et al.*, it was proposed that the decreasing absorption intensity between 220 and 240 nm observed between 20 and 50 ps reflected ClOO vibrational relaxation.[11] To check this hypothesis, we have attempted to reproduce the transient spectra at 20 and 50 ps using the calculated temperature-dependent absorption cross sections of ClOO. In performing this analysis, the experimental spectrum was fit to the expression[11]

$$\Delta A_{\lambda,t} = d_{OClO}\{\varepsilon_{Cl}(\lambda)[Cl(t)] + \varepsilon_{ClO}(\lambda)[ClO(t)]$$
$$+ \varepsilon_{ClOO}(\lambda)[ClOO(t)] - \varepsilon_{OClO}(\lambda)\Delta[OClO]\}. \quad (5)$$

In the above expression, d is the thickness of the sample (0.2 cm) and ε_i are the wavelength-dependent extinction coefficients for the various species of interest. Temporal evolution of the OClO concentration is considered to be complete by 20 ps, in agreement with earlier studies.[26,45] Best reproduction of the 50-ps spectrum [Fig. 8(B)] was obtained with the 298 K absorption spectrum of ClOO, suggesting that this species is vibrationally cold by this time. Surprisingly, the
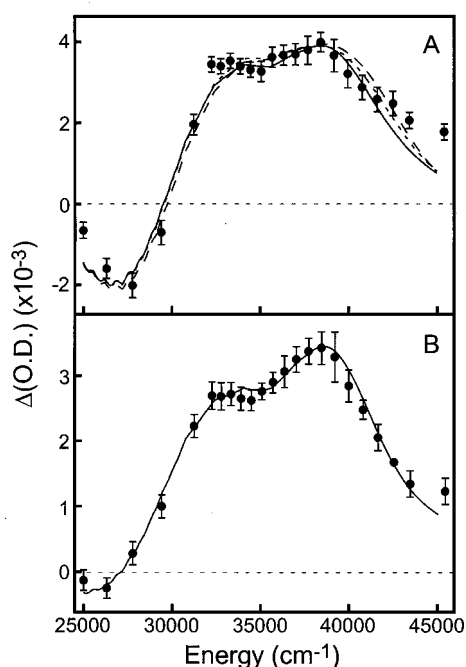
FIG. 8. (A) Fit to the transient absorption spectrum obtained at 20-ps delay reported by Thomsen *et al.* (Ref. 11). The data are given by the points, and the different fits correspond to ClOO molecular temperatures of 298 K (solid line), 700 K (small dash), and 1000 K (long dash). (B) Fit to the transient absorption spectrum obtained at 50-ps delay reported by Thomsen *et al.* (Ref. 11). The data are given by the points and the fit by the solid line. The fit was constructed using the calculated absorption spectrum of ClOO at 298 K as described in the text.

blue edge of the 20-ps spectrum [Fig. 8(A)] could not be satisfactorily reproduced with any of the temperature-dependent ClOO absorption spectra. Reproductions of the transient absorption spectrum at 20 ps using ClOO spectra at 298, 700, and 1000 K are shown in Fig. 8(A). The lower-temperature spectra underestimate the slope of the blue edge, while the spectrum becomes too broad at elevated temperatures. This result suggests that evolution in optical density evident between 220 and 240 nm may not be due exclusively to ClOO (see below).

VI. DISCUSSION

A. ClOO formation and decay

The TRRR results presented here established that ClOO is a photoproduct of OClO in both polar-protic and polar-aprotic environments. Kinetic analysis of the evolution in aqueous ClOO scattering intensity demonstrates that this species appears and decays with time constants of 27.9 ± 4.5 and 398 ± 50 ps, respectively. The appearance time constant derived from TRRR is in excellent agreement with the 21.5 ± 11.2 ps increase in optical density observed at 260 nm [Fig. 6(A)] corresponding to ClOO production. Therefore, these results establish that ClOO appears on the ~ 20-ps timescale in aqueous solution. The 398 ± 50 ps decay time for ClOO determined by TRRR is in agreement with the 251 ± 151 ps production of the Cl–solvent charge–transfer complex measured at 390 nm, and with the 284 ± 70 ps decay time constant observed at 260 nm consistent with ClOO de-

cay. Finally, this time constant is in excellent agreement with the ~ 320 ps decay time constant determined in recent femtosecond pump–probe studies.[11] Therefore, the combined TRRR and pump–probe studies demonstrate that decomposition of ground-state ClOO occurs on the ~ 350 ps timescale.

In freon-11, the TRRR results demonstrate that ClOO is produced with a time constant of 172 ± 30 ps, significantly slower than in water [Fig. 2(C)]. The computational results presented above indicate that vibrational excitation does not drastically affect the ClOO Stokes Raman cross section. This suggests that the solvent-dependent appearance kinetics is not exclusively due to changes in the vibrational relaxation rate, but instead reflects differences in the rate of ground-state ClOO production. We explore this issue in detail in the following section. Quantitative comparison of the ClOO decay dynamics in water and freon-11 is complicated by the fact that decay occurs over times that are comparable with the range of experimentally accessible delays. However, the 864 ± 200 ps decay time for ClOO in freon-11 derived from TRRR suggests that the decomposition of ground-state ClOO is markedly slower in this solvent compared to water. This behavior may reflect increased stability of the Cl–solvent charge–transfer complex formed in water relative to freon-11. Estimates of complex strength using a comparison of complex optical-absorption maxima is compromised by the lack of correlation between this maximum and ionization potential in water as compared to the existence of such a correlation in freon-11.[39] In addition, hydrogen bonding in water might also promote ClOO dissociation by facilitating formation of the Cl–solvent complex.

B. Mechanism of ClOO formation

The results presented here suggest that ClOO production does not occur through geminate recombination of the primary photofragments, but instead occurs through OClO photoisomerization. This conclusion is largely motivated by the similarity in the ClOO production quantum yields in freon-11 and water in contrast to the threefold reduction in geminate recombination efficiency observed in freon-11. This discrepancy suggests that geminate recombination of the primary photoproducts does not result in ground-state ClOO formation. The importance of geminate recombination is also questionable from a kinetic standpoint since the ClOO appearance time constant is two orders of magnitude greater than the subpicosecond time constant for recombination resulting in ground-state OClO production.[26] Therefore, the results presented here can be viewed as supportive of the photoisomerization model. With respect to this model, symmetry arguments suggest that this process occurs through coupling of the $^2B_2$ surface of OClO with one of the $^2A'$ surfaces of ClOO at small bend angles. As demonstrated by Peterson and Werner, these two surfaces correlate by symmetry, and a symmetric ClOO structure can be supported on the $^2B_2$ surface.[23] This structure is highly bent, with a corresponding OClO angle of 50°. A similar mechanism was proposed by Gole, who suggested that isomerization of OClO to ClOO

proceeds via a strong vibronic coupling between the $^2A_1$ and $^2B_2$ states of OClO which correlate with the $^2A'$ state of ClOO.[22]

As discussed above, the ClOO appearance kinetics are solvent dependent, and the computational studies presented here suggest that this behavior reflects a variation in the rate of ground-state ClOO production. This variation most likely arises from the alteration of state energetics with solvent polarity. Freon-11 possesses a modest dipole moment (0.46 D) relative to water (1.85 D); therefore, differential solvation of the ClOO ground-and/or excited states may alter the state energetics and subsequently the internal conversion rate. Support for this hypothesis would be solvatochromic behavior of the ClOO absorption band. Unfortunately, such information is unavailable since the absorption spectrum of ClOO has only been reported in highly polar environments.

C. Mechanism of Cl production in OClO

Earlier pump–probe work has shown that for aqueous OClO, Cl formation is a bifurcated process where the majority (80%) of Cl is formed with a time constant of ~6 ps while the remainder (20%) is formed on the ~100-ps time scale. The later-time production of Cl arises from the ground-state decomposition of ClOO as described above.[11,16] Therefore, the question remains as to the mechanism for fast or ''prompt'' Cl production. This photoproduct channel has been assigned to direct dissociation of OClO via the bending coordinate.[4,23,46] However, 6 ps is rather slow for direct dissociation, and recent studies suggest that internal conversion of the optically prepared excited state occurs in ~200 fs in aqueous solution.[47] Therefore, we outline here an alternative mechanism for Cl production. As discussed above, a fraction of photoexcited OClO undergoes photoisomerization on the $^2B_2$ surface to produce ClOO in an excited $^2A'$ state.[34] We propose that the majority of ClOO continues along the reaction coordinate and forms a distorted intermediate resembling the Cl and O_2 photofragments, and that this intermediate undergoes dissociation into Cl and O_2 with a time constant of 6 ps. A similar intermediate structure was invoked to explain early-time transient absorption intensity in the UV,[9] and may also be responsible for a portion of the intensity observed between 220 and 240 nm in the 20-ps transient absorption spectrum (Fig. 8).[11] The remainder of excited-state ClOO undergoes internal conversion to the $^2A''$ ground state and subsequent decomposition into Cl and O_2. This model rests on the assumption that bifurcation of the Cl production channels occurs on a lower-energy excited state, allowing for both prompt Cl production as well as the formation of ground-state ClOO. One difficulty with this mechanism is that *ab initio* studies predict that all ClOO excited states are dissociative.[34] However, similar calculations in the condensed phase have not been performed. In the presence of solvent, these surfaces might be modified to allow for the formation of a stable, excited-state ClOO. In support for this hypothesis, recent *ab initio* work has shown that asymmetric distortions of the $^2B_2$ surface that lead to symmetry breaking (C_{2v} to C_s) favor an increase in the well depth of the $^2A'$ state of ClOO.[23] However, in the gas phase this state is bound by no more than 0.2 eV with respect to Cl

and O_2 dissociation. Clearly, evaluation of this model is entirely dependent on ascertaining the nature of these lower-energy excited states.

VII. CONCLUSION

In this manuscript, we have presented TRRR studies of ClOO production following OClO photoexcitation in water and freon-11. Aqueous ClOO appears and decays with time constants of 27.9 ± 4.5 and 398 ± 50 ps, respectively. In freon-11, the ClOO kinetics are much slower, with appearance and decay time constants of 172 ± 30 and $\sim 864 \pm 200$ ps, respectively. We have shown that that the quantum yield for ClOO production is similar in these solvents, yet the geminate recombination quantum yield is substantially reduced in freon-11 relative to water. These two results preclude geminate recombination as the mechanism of ClOO formation. Instead, photoisomerization of OClO followed by excited-state internal conversion was proposed to result in ground-state ClOO formation. Once formed, ground-state ClOO undergoes thermal decomposition to form Cl and O_2 on the subnanosecond time scale, with the rate of this decomposition being solvent dependent. The results presented here provide a better understanding of the mechanism of both ClOO and Cl production.

[1] V. Vaida and J. D. Simon, Science **268**, 1443 (1995).
[2] P. J. Reid, Acc. Chem. Res. **34**, 691 (2001).
[3] T. Wagner, C. Leue, K. Pfeilsticker, and U. Platt, J. Geophys. Res. **106**, 4971 (2001).
[4] H. F. Davis and Y. T. Lee, J. Phys. Chem. **96**, 5681 (1992).
[5] W. G. Lawrence, K. C. Clemitshaw, and V. A. Apkarian, J. Geophys. Res. **95**, 18591 (1990).
[6] A. Arkell and I. Schwager, J. Am. Chem. Soc. **89**, 5999 (1967).
[7] H. S. P. Müller and H. Willner, J. Phys. Chem. **97**, 10589 (1993).
[8] R. C. Dunn, B. N. Flanders, and J. D. Simon, J. Phys. Chem. **99**, 7360 (1995).
[9] J. Thogersen, P. U. Jepsen, C. L. Thomsen, J. A. Poulsen, J. R. Byberg, and S. R. Keiding, J. Phys. Chem. A **101**, 3317 (1997).
[10] M. J. Philpott, S. Charalambous, and P. J. Reid, Chem. Phys. Lett. **281**, 1 (1997).
[11] C. L. Thomsen, P. J. Reid, and S. R. Keiding, J. Am. Chem. Soc. **122**, 12795 (2000).
[12] G. Porter and F. J. Wright, Discuss. Faraday Soc. **14**, 23 (1953).
[13] M. M. Rochkind and G. C. Pimentel, J. Chem. Phys. **46**, 4481 (1967).
[14] K. A. Peterson and H.-J. Werner, J. Chem. Phys. **96**, 8948 (1992).
[15] C. J. Pursell, J. Conyers, P. Alapat, and R. Parveen, J. Phys. Chem. **99**, 10433 (1995).
[16] C. L. Thomsen, M. P. Philpott, S. C. Hayes, and P. J. Reid, J. Chem. Phys. **112**, 505 (2000).
[17] V. Vaida, S. Solomon, E. C. Richard, E. Ruhl, and A. Jefferson, Nature (London) **342**, 405 (1989).
[18] E. Ruhl, A. Jefferson, and V. Vaida, J. Phys. Chem. **94**, 2990 (1990).
[19] Y. J. Chang and J. D. Simon, J. Phys. Chem. **100**, 6406 (1996).

[20] K. Johnsson, A. Engdahl, P. Ouis, and B. Nelander, J. Phys. Chem. **96**, 5778 (1992).

[21] M. P. Gane, N. A. Williams, and J. R. Sodeau, J. Chem. Soc., Faraday Trans. **93**, 2747 (1997).

[22] J. L. Gole, J. Phys. Chem. **84**, 1333 (1980).

[23] K. A. Peterson and H.-J. Werner, J. Chem. Phys. **105**, 9823 (1996).

[24] K. A. Peterson, J. Chem. Phys. **109**, 8864 (1998).

[25] P. K. Walhout, J. C. Alfano, K. A. M. Thakur, and P. F. Barbara, J. Phys. Chem. **99**, 7568 (1995).

[26] S. C. Hayes, M. P. Philpott, S. G. Mayer, and S. G. Reid, J. Phys. Chem. A **103**, 5534 (1999).

[27] M. J. Philpott, S. C. Hayes, and P. J. Reid, Chem. Phys. **236**, 207 (1998).

[28] S. C. Hayes, M. J. Philpott, and P. J. Reid, J. Chem. Phys. **109**, 2596 (1998).

[29] C. E. Foster and P. J. Reid, J. Phys. Chem. A **102**, 3541 (1998).

[30] A. Esposito, C. Foster, R. Beckman, and P. J. Reid, J. Phys. Chem. A **101**, 5309 (1997).

[31] S.-Y. Lee and E. J. Heller, J. Chem. Phys. **71**, 4777 (1979).

[32] A. B. Myers and R. A. Mathies, in *Biological Applications of Raman Spectroscopy: Vol. 2—Resonance Raman Spectra of Polyenes and Aromatics*, edited by T. G. Spiro (Wiley, New York, 1987).

[33] J. Sue and S. Mukamel, J. Chem. Phys. **88**, 651 (1987).

[34] J. A. Jafri, B. H. Lengsfield III, and D. H. Phillips, J. Chem. Phys. **83**, 1693 (1985).

[35] M. D. Feit, J. A. Fleck, and A. Steiger, J. Comput. Phys. **47**, 412 (1982).

[36] M. D. Feit and J. A. Fleck, J. Chem. Phys. **78**, 301 (1983).

[37] G. R. Loppnow and R. A. Mathies, Biophys. J. **54**, 35 (1988).

[38] K. Johnsson, A. Engdahl, P. Ouis, and B. Nelander, J. Mol. Struct. **293**, 137 (1993).

[39] J. E. Chateauneuf, Chem. Phys. Lett. **164**, 577 (1989).

[40] R. L. Mauldin III, J. B. Burkholder, and A. R. Ravishankara, J. Phys. Chem. **96**, 2582 (1992).

[41] B. Li and A. B. Myers, J. Phys. Chem. **94**, 4051 (1990).

[42] M. Moskovits and K. H. Michaelian, J. Chem. Phys. **69**, 2306 (1978).

[43] The depolarization ratio used was 0.18, equivalent to the one measured at 282 nm (Ref. 29).

[44] S. Baer, H. Hippler, R. Rahn, M. Siefke, N. Seitzinger, and J. Troe, J. Chem. Phys. **95**, 6463 (1991).

[45] J. Thogersen, C. L. Thomsen, J. A. Poulsen, and S. R. Keiding, J. Phys. Chem. A **102**, 4186 (1998).

[46] H. F. Davis and Y. T. Lee, J. Chem. Phys. **105**, 8142 (1996).

[47] S. C. Hayes, C. C. Cooksey, P. M. Wallace, and P. J. Reid, J. Phys. Chem. **105**, 9819 (2001).